Catalysis Science & Technology

ROYAL SOCIETY OF CHEMISTRY

PAPER

View Article Online
View Journal | View Issue

Open Access Article. Published on 07 November 2022. Downloaded on 2/12/2026 5:12:10 AM.
This article is licensed under a Creative Commons Attribution 3.0 Unported Licence.

Check for updates

Cite this: *Catal. Sci. Technol.*, 2022, **12**, 7433

Received 19th September 2022,
Accepted 5th November 2022

DOI: 10.1039/d2cy01638a

rsc.li/catalysis

In situ formation of $Ni(CO)_4$ contaminant during IR analyses using a metal-containing reaction cell

Frederic C. Meunier

The formation of ppm levels of volatile $Ni(CO)_4$ occurred in the presence of 1 kPa CO over a worn commercial cell used for diffuse reflectance FT-IR, but not on a more recent cell. The presence of $Ni(CO)_4$ led to nickel deposition on Au and Cu-based catalysts evidenced by the presence of specific Ni–CO IR bands. In contrast, no Ni–CO IR bands could be observed on plain silica, suggesting that specific sites are required to decompose $Ni(CO)_4$. The unambiguous evolution of the carbonyl signal on Au/SiO_2 could be used as a test to assess the presence of ppm levels of $Ni(CO)_4$ in *in situ* and *operando* IR cells.

Nickel tetracarbonyl was discovered by Mond *et al.* in 1890 (ref. 1) and is at the core of the Mond process used for nickel refining.[2] The nickel ore is first reduced with hydrogen and then exposed to carbon monoxide at temperatures around 50 °C to produce the highly volatile $Ni(CO)_4$ (eqn (1) and (2)). The latter step allows separating Ni from the other elements present in the ore. The maximum rate of formation of $Ni(CO)_4$ is actually around 130 °C and favored by higher CO pressures.[3] The collected $Ni(CO)_4$ is then heated up at temperatures between 200–250 °C, where it decomposes into CO and Ni^0 (eqn (3)).

$$NiO + H_2 \rightarrow Ni + H_2O, \quad T > 300\ ^\circ C \tag{1}$$

$$Ni + CO \rightarrow Ni(CO)_4, \quad 20\ ^\circ C < T < 180\ ^\circ C \tag{2}$$

$$Ni(CO)_4 \rightarrow Ni + 4CO, \quad T > 200\ ^\circ C \tag{3}$$

The Mond process is yet only used when high purity nickel is sought, because of the acute toxicity[4,5] of this compound. In spite of its toxicity, $Ni(CO)_4$ is routinely used in laboratories to prepare organometallic complexes[6] and thin films.[7]

The description of the Mond process emphasizes that $Ni(CO)_4$ may form whenever Ni-based catalysts are reduced and exposed to CO at temperatures below 200 °C. In fact, Hadjiivanov and co-workers[8] showed that $Ni(CO)_4$ formed already at −188 °C when SiO_2-supported Ni nanoparticles (about 4 nm in diameter) were exposed to 0.2 kPa of CO. This compound remained physisorbed up to −40 °C, displaying an IR band at 2048 cm^{-1} (Table 1). Gaseous $Ni(CO)_4$ (2058 cm^{-1}) was released when the temperature was further increased.

Univ Lyon, Université Claude Bernard Lyon, CNRS, IRCELYON, 2 Av. Albert Einstein, 69626 Villeurbanne, France. E-mail: fcm@ircelyon.univ-lyon1.fr

The corrosion rate of Ni nanoparticles typically increases with lower coordinations of the Ni atoms[8] and high CO surface coverages,[12,13] as Ni has to be coordinated by four CO molecules to form $Ni(CO)_4$. Adsorbed carbon, formed through CO dissociation or disproportionation catalyzed by Ni, limits this rate and has hindered the understanding of the processes taking place at Ni surfaces.[13]

It is reasonable to propose that in most (if not all cases) the adsorption of CO on Ni nanoparticles around room temperature will inevitably result in the formation of some gaseous or adsorbed $Ni(CO)_4$. In view of the discussion above, the use of CO as reactant or molecular probe on metallic Ni nanoparticles should be restricted to temperatures above 200 °C to prevent the corrosion of the metal and dissemination of Ni compounds in reactor lines and exhaust gases.

Yet, Pereira and Martin[11] exposed a Ni/SiO_2 catalysts to 1 kPa of CO at 25 °C, reporting various adsorbed species observed by IR, such as subcarbonyls Ni–$(CO)_{2\ or\ 3}$ at 2082 cm^{-1}, linear Ni–CO at 2040 cm^{-1} and bridged Ni_2–CO at 1920 cm^{-1}, but not $Ni(CO)_4$.

Mirodatos and co-workers[14] exposed a Ni/SiO_2 to 1 kPa of CO at room temperature and observed all the carbonyl species aforementioned, including adsorbed $Ni(CO)_4$ with a band at around 2045 cm^{-1}. Ni tetracarbonyl and subcarbonyls were proposed to be instrumental in the sintering of Ni nanoparticles, by facilitating the transport of Ni atoms from small to larger particles (Ostwald ripening).[14,15]

Derrouiche and Bianchi[16] adsorbed 1 or 2 kPa of CO between room temperature and 340 °C on Ni/Al_2O_3 catalysts. These authors reported important modifications (restructuring) of the Ni surface, but did not mention the possible corrosion by $Ni(CO)_4$, while Ni subcarbonyls were present. The disproportionation of CO leading to carbon deposition was also observed. The heat of adsorption at zero coverage of linear and bridged CO were found to be both

Open Access Article. Published on 07 November 2022. Downloaded on 2/12/2026 5:12:10 AM.
This article is licensed under a Creative Commons Attribution 3.0 Unported Licence.

Table 1 Vibration wavenumber of CO in various molecules and adsorbates

Species	Wavenumber (cm^{-1})	Ref.
Gaseous $Ni(CO)_4$	2058	8
Physisorbed $Ni(CO)_4$	2048	8
Ni_2–CO (bridged CO)	1950–1900	8–11
Ni–$(CO)_{2\ or\ 3}$ (subcarbonyl)	2080–2050	8, 11, 14
Ni–CO on Ni nanoparticles or Ni–Cu alloys, from high to low coverages	2050–1995	9, 11, 14
Au–CO on Au metallic nanoparticles	2120–2100	25, 26
Cu–CO on Cu metallic nanoparticles	2110–2080	27

around 150 kJ mol^{-1}, stressing that CO adsorption is very strong on metallic Ni. Adsorption isobars indicated essentially full CO coverage up to 300 °C.

IR spectra collected on Ni nanoparticles at 300 °C under CO/He (ref. 16) or CO/H_2 (ref. 10 and 16) (methanation conditions) exhibited a strong band of linear CO at *ca.* 2050 cm^{-1}. The presence of adsorbed or gaseous $Ni(CO)_4$ at these temperatures can be safely excluded. This observation stress the difficulty in discriminating bands in the 2060–2040 cm^{-1} region at low temperatures, as those could be assigned both to $Ni(CO)_4$ (gaseous or adsorbed) and linearly adsorbed Ni–CO (Table 1).

Another insidious aspect of $Ni(CO)_4$ is that it can arise from the experimental setup and contaminate initially Ni-free samples. We commented[17] on a study by Zheng *et al.*[18] dealing with the reactivity of CO over Ni-free mixed oxides of CeO_2 and ZrO_2. We concluded that that their feed had been contaminated with $Ni(CO)_4$, as evidenced by the presence of a band near 2055 cm^{-1} (Fig. 1) (note: the typical precision on wavenumbers is ±2 cm^{-1}). This contaminant eventually led to the deposition of Ni nanoparticles over ceria, explaining the broader bands centered at 2007 cm^{-1}, that should be assigned to CO adsorbed on metallic Ni nanoparticles and not to any CO adsorbed on ceria as had been proposed by Zheng *et al.*[18]

The concentration of $Ni(CO)_4$ appeared to be quite high in view of the relative intensities of the CO(g) signal (CO pressure = 1 kPa) and that of $Ni(CO)_4$. Assuming that the molar extinction coefficient of the CO(g) band and that of each carbonyl ligand in $Ni(CO)_4$ are identical, the approximate concentration of $Ni(CO)_4$ was about 0.3 kPa.

$Ni(CO)_4$ can also be formed *in situ*, for instance inside a spectroscopic cell whose steel had been corroded by NO_x, as we reported earlier in a paper retractation.[19] The formation of $Ni(CO)_4$ was actually only observed if the cell had been brought above 300 °C under H_2, so that the oxidized nickel present could be reduced to the metallic state, and then exposed to CO at low temperature, to favor multiple CO adsorption on Ni^0 and $Ni(CO)_4$ formation. The presence of O_2 also prevented the contamination, likely due to the passivation of metallic nickel through oxidation. The corrosion of Ni^0 by CO can occur at temperatures as low as −188 °C as aforementioned[8] and is likely to be a problem more common than thought, as suggested in a recent paper.[20]

The present contribution aims at describing explicitly the main observations reported on a 1 wt% Au/SiO_2 discussed in our earlier retractation note, as well as providing additional data collected on 6 wt% Cu/ZrO_2. It will be shown that $Ni(CO)_4$ will be observed only in the case of the corroded cell, leading to modifications of the DRIFTS spectra collected over both supported metals. It will also be noted that a support like silica does not lead to the formation of visible Ni carbonyl adsorbate bands, while exposed to $Ni(CO)_4$.

The preparation method and detailed characterization of the 1 wt% Au/SiO_2 (ref. 21) and 6 wt% Cu/ZrO_2 (ref. 22) were detailed in the earlier references. In brief, the silica support was a commercial (Zeosil, surface area of 175 m^2 g^{-1}), which was first functionalized by grafting APTMS (3-aminopropyltrimethoxysilane) according to a method reported elsewhere.[23] Monoclinic ZrO_2 (surface area of 131 m^2 g^{-1}) was

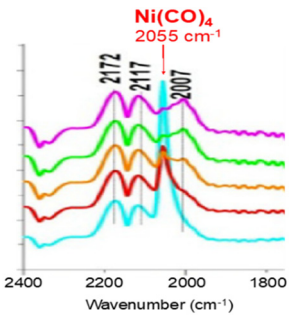

Fig. 1 *In situ* DRIFTS spectra recorded over ceria under 1 kPa CO (bands at 2172 and 2117 cm^{-1}) showing the presence of Ni(CO)4 (band at 2055 cm^{-1}) (adapted from ref. 17 with permission, © 2019 Elsevier B. V.).

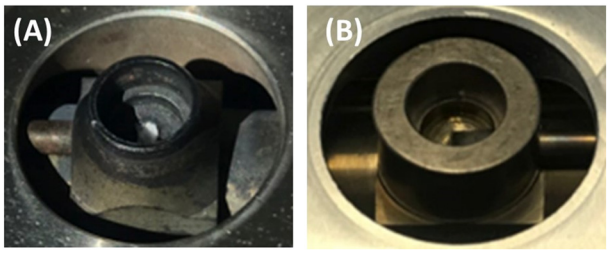

Fig. 2 Pictures of the crucibles of the Harrick high temperature reaction chambers: (A) older cell previously used with NO_x and (B) newer cell.

Open Access Article. Published on 07 November 2022. Downloaded on 2/12/2026 5:12:10 AM.
This article is licensed under a Creative Commons Attribution 3.0 Unported Licence.

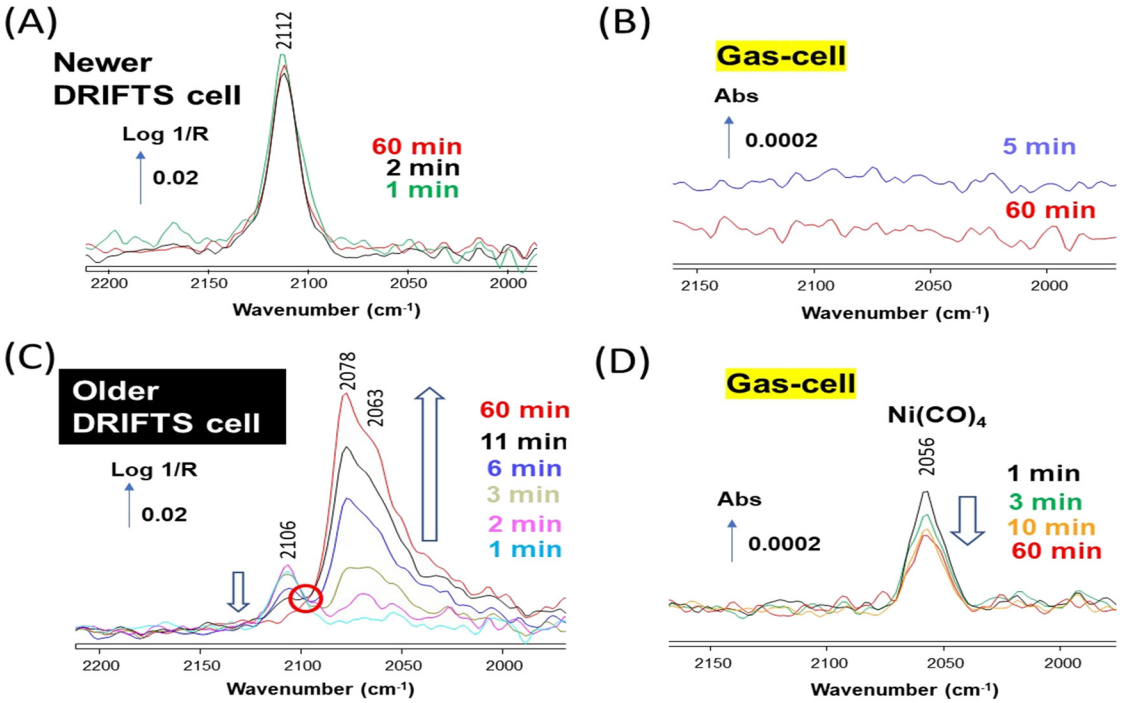

Fig. 3 (A) *In situ* DRIFTS spectra recorded over Au/SiO_2 under 1% CO/He at 50 °C at various times in the newer DRIFTS cell. (B) Corresponding transmission IR spectra of the effluents from the newer DRIFTS cell showing no compounds, except for CO(g) whose spectrum had been subtracted. (C) *In situ* DRIFTS spectra recorded over Au/SiO_2 under 1% CO/He at 50 °C at various times in the older DRIFTS cell. (D) Corresponding transmission IR spectra of the effluents from the older DRIFTS cell showing the presence of $Ni(CO)_4$. The contribution of gas-phase CO was subtracted for both DRIFTS and transmission IR spectra.

obtained from MEL Chemicals. The metals were added using wet impregnation of $Cu(NO_3)_2$ and $HAuCl_4{\cdot}3H_2O$. High purity He (99.999%), H_2 (99.999%) and 5% CO/He were supplied by Air Liquide. The gas stream was further purified by using a cold trap set at liquid nitrogen temperature.

The Diffuse Reflectance FT-IR (DRIFTS) Praying Mantis assembly from Harrick was used and placed in a Bruker TENSOR 27 spectrometer fitted with a DTGS detector. DRIFTS spectra were recorded at 50 °C, following reduction in 50% H_2/He of the samples for 30 min at 300 and 350 °C for the Au/SiO_2 and Cu/ZrO_2, respectively. The DRIFTS background was recorded at 50 °C under He after sample reduction, just before introducing CO. The DRIFTS cell effluent was analyzed by transmission IR using a 10 cm-pathlength gas cell (from Harrick) kept at 65 °C, located in a Bruker TENSOR 27 spectrometer fitted with a DTGS detector.

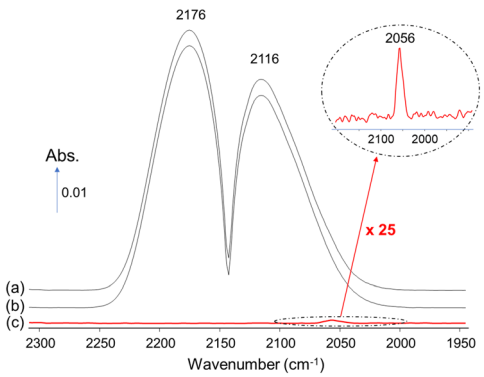

Fig. 4 Transmission IR spectra of a stream made of 1% CO/He (a) after passing through the reduced older DRIFTS cell and (b) by-passing the cell. (c) Difference spectrum (a) and (b) showing the spectrum of $Ni(CO)_4$.

Fig. 2 shows a picture of the DRIFTS cells used, which were both bought from Harrick and made of 316 stainless-steel (Praying Mantis™ High Temperature Reaction Chamber).[24] The older cell (Fig. 2A) had been used earlier with NO–O_2 mixtures and presented clear signs of wearing, in contrast to the newer cell (Fig. 2B).

The Au/SiO_2 sample was first investigated using the newer DRIFTS cell. The sample was reduced *in situ* at 300 °C and then exposed to 1% CO/He at 50 °C. A single band at 2112 cm^{-1} was observed, which was stable over 60 min (Fig. 3A). This band is assigned to CO adsorbed on low coordination sites (*e.g.*, edges and corners) of Au nanoparticles.[25,26] The newer DRIFTS cell effluent, which was monitored using a transmission gas-cell directly located after the DRIFTS cell, showed no other bands than those of gas-phase CO (Fig. 3B, the contribution of CO(g) was subtracted).

The Au/SiO_2 sample was then investigated using the older DRIFTS cell, applying the same experimental procedure. A band at 2106 cm^{-1} was initially observed, also assigned to CO adsorbed on Au low coordination sites (Fig. 3C). In contrast to the case of the newer cell, the IR signal rapidly evolved. The intensity of the Au–CO band gradually disappeared, while large bands around 2078–2063 cm^{-1} were formed. The

Open Access Article. Published on 07 November 2022. Downloaded on 2/12/2026 5:12:10 AM.
This article is licensed under a Creative Commons Attribution 3.0 Unported Licence.

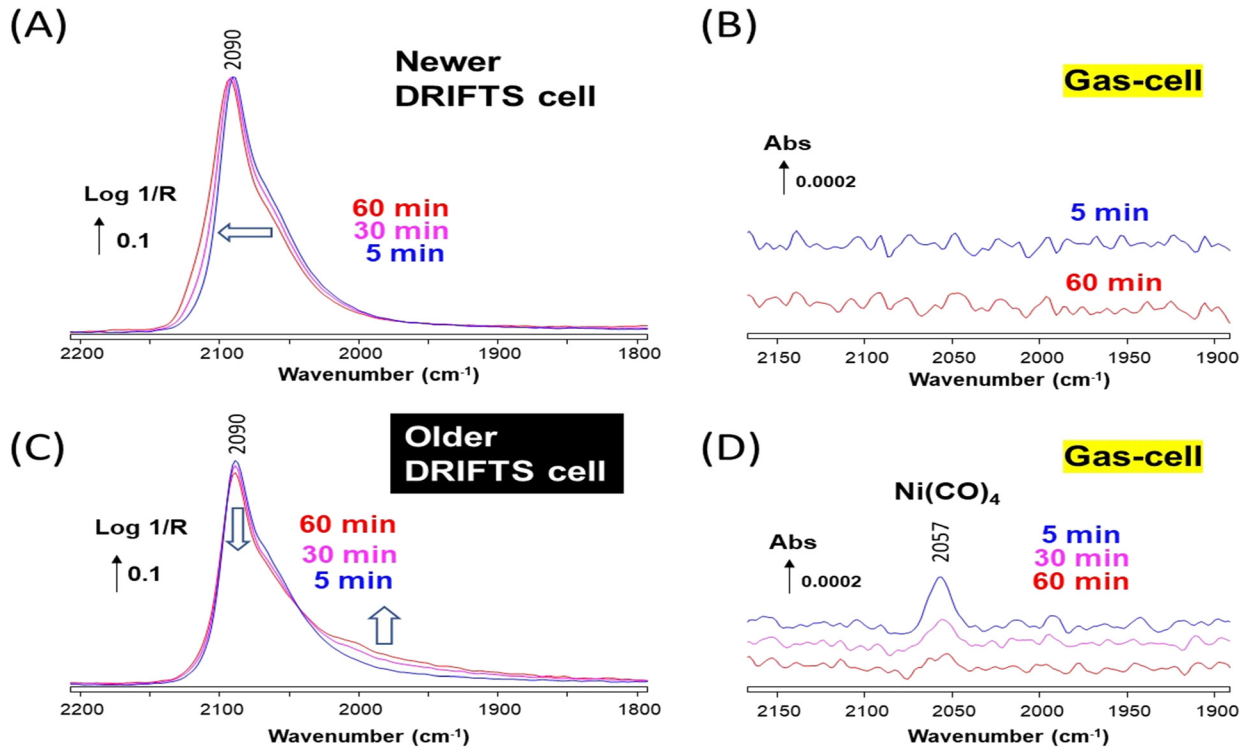

Fig. 5 (A) *In situ* DRIFTS spectra recorded over Cu/ZrO_2 under 1% CO/He at 50 °C at various times in the newer DRIFTS cell. (B) Corresponding transmission IR spectra of the effluents from the newer DRIFTS cell showing no compounds, except for CO(g) whose spectrum had been subtracted. (C) *In situ* DRIFTS spectra recorded over Cu/ZrO_2 under 1% CO/He at 50 °C at various times in the older DRIFTS cell. (D) Corresponding transmission IR spectra of the effluents from the older DRIFTS cell showing the presence of $Ni(CO)_4$. The contribution of gas-phase CO was subtracted for both DRIFTS and transmission IR spectra.

two processes appeared correlated as an isosbestic point around 2100 cm^{-1} was observed (circled in red in Fig. 3C). The older DRIFTS cell effluent showed a clear band at 2056 cm^{-1} over the whole duration of the experiment, which can be assigned to the gaseous compound $Ni(CO)_4$ (ref. 8) (Fig. 3D, the contribution of CO(g) was subtracted).

This set of experiment confirms our earlier retractation paper[19] and the work by Yao *et al.*[20] that the evolution of the Au–CO signal from a band at 2110 cm^{-1} towards one at *ca.* 2070 cm^{-1} was related to the presence of traces of $Ni(CO)_4$. Note that in neither contributions had the actual observation of gaseous $Ni(CO)_4$ bands been reported. The bands around 2070 cm^{-1} are due to nickel carbonyl species, likely subcarbonyls $Ni(CO)_{2\ or\ 3}$ (Table 1), present at the surface of the Au–Ni alloy formed. The total disappearance of the Au–CO signal at 2106 cm^{-1} indicated that Ni eventually occupied the corresponding sites, *i.e.*, edges and corners of the alloy nanoparticles.

Our data also show that the $Ni(CO)_4$ was formed *in situ* on the older cell walls, as our 1% CO/He feed was free of any $Ni(CO)_4$ as demonstrated by the absence of bands below 2100 cm^{-1} in the case of the experiments carried out with the newer DRIFTS cell (Fig. 3A and B).

It is also important to stress that $Ni(CO)_4$ was only observed if a reductive treatment had been performed in the older cell (data not shown). This observation indicates that the Ni present on the cell walls needed to be reduced to the metallic state to be able to form the tetracarbonyl compounds, similarly to the Mond process (eqn (1)–(3)). This also explains why $Ni(CO)_4$ cannot be observed when co-feeding CO and O_2, since the latter readily oxidises Ni^0.

The difficulty in spotting the gas-phase signal of $Ni(CO)_4$, which overlaps with that of CO, is exemplified in Fig. 4. The spectrum of 1% CO/He stream recorded after passing through the "reduced" older DRIFTS (Fig. 4a) and that obtained by-passing the cell (Fig. 4b) both essentially displayed the typical rovibrational spectrum of CO. The spectrum obtained by subtracting the latter from the former evidences the presence of $Ni(CO)_4$ in the case of the older cell (Fig. 4c). It is clear that the actual concentration of $Ni(CO)_4$ formed was far lower than that of CO. The approximate concentration of $Ni(CO)_4$ was about 4 ppm, assuming that the molar extinction coefficient of the CO(g) band and that of each carbonyl ligand in $Ni(CO)_4$ are identical. Such weak gas-phase signals are hard to spot if not carefully sought. It is thus worth noting the greater sensitivity of the DRIFTS method on Au/SiO_2 (Fig. 3C), which appears as a suitable means to evidence the presence of contamination by Ni carbonyls.

Similar experiments were carried out over a Cu/ZrO_2 sample. The sample reduced at 350 °C then exposed to 1% CO/He at 50 °C in the newer cell exhibited a strong band at

Open Access Article. Published on 07 November 2022. Downloaded on 2/12/2026 5:12:10 AM.
This article is licensed under a Creative Commons Attribution 3.0 Unported Licence.

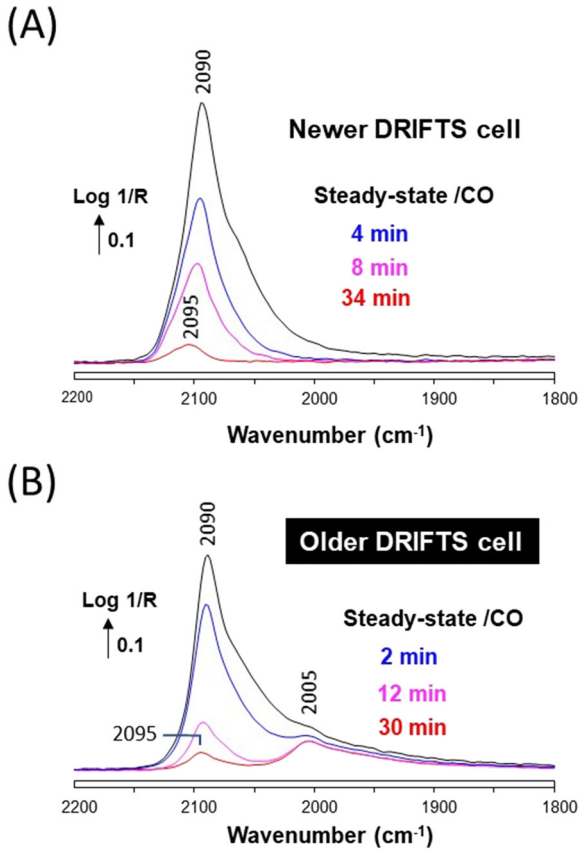

Fig. 6 (A) *In situ* DRIFTS spectra recorded in the newer cell over Cu/ZrO_2 under a He stream at 50 °C and various times after removing CO. (B) Same recorded in the older DRIFTS cell.

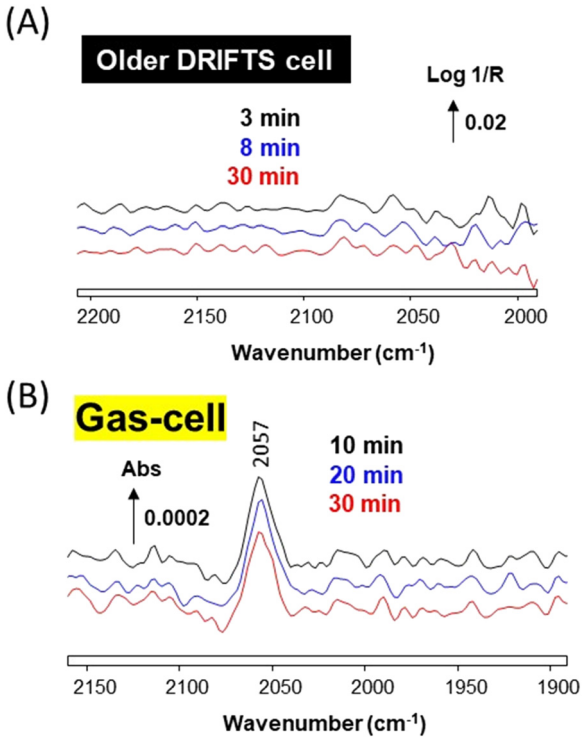

Fig. 7 (A) *In situ* DRIFTS spectra recorded over SiO_2 under 1% CO/He at 50 °C at various times in the older DRIFTS cell. (B) Corresponding transmission IR spectra of the effluents from the older DRIFTS cell showing the presence of $Ni(CO)_4$. The contribution of gas-phase CO was subtracted.

2090 cm^{-1} (Fig. 5A), assigned to CO adsorbed on metallic Cu nanoparticles.[27] The asymmetry of the band indicated that various sites and particles sizes were present. The shape of the DRIFTS band gradually evolved over time, which is only assigned to particle reconstruction, since no nickel carbonyl could be observed over the duration of the experiment (Fig. 5B). The global shift towards higher wavenumbers of the band shoulder suggests that the surface was becoming more defective in the presence of CO.[27]

The same Cu/ZrO_2 sample studied in the older DRIFTS cell showed initially an essentially identical band at 2090 cm^{-1} (Fig. 5C), but this time $Ni(CO)_4$ was observed in the cell effluent (Fig. 5D). The DRIFT also evolved, but in a different manner as compared to the case of the newer cell. The band maximum decreased in intensity and a shoulder grew on the low wavenumber side, below 2050 cm^{-1}.

The evolution of the DRIFTS band following the removal of CO was monitored to better ascertain the differences brought about by the presence of $Ni(CO)_4$ on Cu/ZrO_2. A significant difference in the desorption rates of CO from Cu and Ni is expected, since the heat of adsorption is significantly different on these two metals (*ca.* around 82 kJ mol^{-1} for Cu–CO (ref. 28) and 150 kJ mol^{-1} for Ni–CO (ref. 16)). The band intensity rapidly decreased and blue-shifted from 2090 to 2095 cm^{-1} in the case of the Ni-free newer cell (Fig. 6A). This type of carbonyl band decay is typical of Cu nanoparticles.[27] The same behavior of the main Cu–CO band at 2090 cm^{-1} was observed in the case of the Ni-contaminated older cell, but the Ni-related shoulder was stable and clearly appeared as a band located at 2005 cm^{-1} (Fig. 6B). Such stable signal at 2005 cm^{-1} is typical of Ni–CO (linear monocarbonyl), either on pure Ni or Ni–Cu alloys.[9,11] These data thus clearly show that some Ni atoms have been deposited at the surface of the Cu/ZrO_2 material in the case of using the older DRIFTS cell.

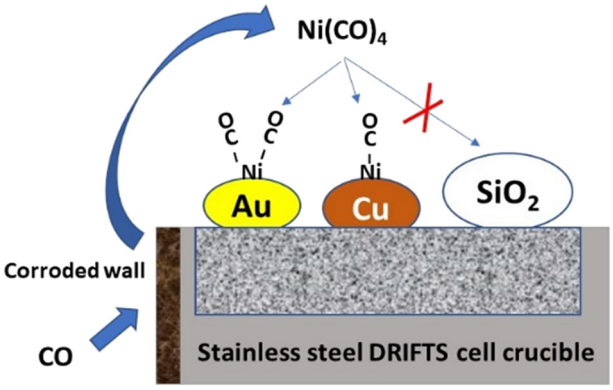

Fig. 8 Schematic representation of the contamination from $Ni(CO)_4$ and species formed on various solids.

Open Access Article. Published on 07 November 2022. Downloaded on 2/12/2026 5:12:10 AM.
This article is licensed under a Creative Commons Attribution 3.0 Unported Licence.

Another experiment was conducted over plain silica, to determine whether or not $Ni(CO)_4$ would decompose on a simple oxide. SiO_2 (from the same batch used to prepare the Au/SiO_2 catalyst) was reduced *in situ* at 300 °C and then exposed to CO in both the newer cell (data not shown) and the older cell (Fig. 7). In both cases no Ni carbonyl surface bands could be observed by DRIFTS (Fig. 7A), despite the fact that $Ni(CO)_4$ bands could be observed in the effluent of the older cell (Fig. 7B). This stresses that some specific catalytic sites are required to decompose $Ni(CO)_4$ at 50 °C, such as those found on Au or Cu nanoparticles, while plain silica is unable to carry out this decomposition. Zecchina and co-workers[29] have reported that strong Lewis sites of alumina were able to decompose $Ni(CO)_4$ by decarbonylation, albeit slowly at 50 °C.

It must be stressed that iron pentacarbonyl $Fe(CO)_5$ was not observed (this compound is characterized by two strong IR bands at 2024 and 2000 cm^{-1}).[30] This observation may be rationalized by the fact that any iron oxide present at the surface of the corroded older cell is harder to reduce that NiO. In fact, Popov *et al.*[31] reported reduction temperatures of 420 °C and 560 °C for NiO and Fe_2O_3, respectively.

In conclusion, if was shown that a corroded stainless steel DRIFTS cell can lead to the formation of ppm levels of $Ni(CO)_4$. This contaminant will decompose on Au to lead to a clear new set of Ni subcarbonyl bands and to a shoulder of Ni monocarbonyl on Cu (Fig. 8). No decomposition was observed at 50 °C on plain silica, stressing that specific metallic (or Lewis acid[29]) sites are required to enable decarbonylation under these conditions. We propose that IR monitoring of Au/SiO_2 could be used as a test to characterise the presence of trace amounts of $Ni(CO)_4$, because of its high sensitivity and clarity in the interpretation of the corresponding IR spectrum. The Au–CO signal is stable around 2110 cm^{-1} in the absence of $Ni(CO)_4$, while new Ni–$(CO)_x$ bands are formed below 2080 cm^{-1} in its presence. Such simple discrimination is not possible in the cases of most other metal carbonyls, which all already present bands below 2080 cm^{-1}.

Author contributions

FCM designed the project and carried out the experiments and analysis and wrote the manuscript.

Conflicts of interest

There are no conflicts to declare.

Acknowledgements

Anaelle Paredes-Nunez and Taha Elgayyar are acknowledged for the preparation of the Cu/ZrO_2 and Au/SiO_2, respectively.

Notes and references

1 L. Mond, C. Langer and F. Quincke, *J. Chem. Soc., Trans.*, 1890, **57**, 749–753.
2 https://en.wikipedia.org/wiki/Mond_process.
3 K. Lascelles, L. G. Morgan, D. Nicholls and D. Beyersmann, *Ullmann's Encyclopedia of Industrial Chemistry*, Weinheim: Wiley-VCH, DOI: 10.1002/14356007.a17_235.pub2.
4 F. W. Sunderman, C. L. Range, F. W. Sunderman Jr., A. J. Donnelly and G. W. Lucyszyn, *Am. J. Clin. Pathol.*, 1961, **36**, 477–491.
5 Z. Shi, *Sci. Total Environ.*, 1994, **148**, 293–298.
6 M. Keßler, L. Hartmann, H.-G. Stammler, B. Neumann, G.-V. Röschenthaler and B. Hoge, *Inorg. Chem.*, 2022, **61**, 10833–10843.
7 M. Smolarek, H. Kierzkowska-Pawlak, R. Kapica, M. Fronczak, M. Sitarz, M. Leśniak and J. Tyczkowski, *Catalysts*, 2021, **11**, 905.
8 M. Mihaylov, K. Hadjiivanov and H. Knozinger, *Catal. Lett.*, 2001, **76**, 59–63.
9 Y. Yao and D. W. Goodman, *Phys. Chem. Chem. Phys.*, 2014, **16**, 3823–3829.
10 D. Lorito, H. Li, A. Travert, F. Maugé, F. C. Meunier, Y. Schuurman and C. Mirodatos, *Catal. Today*, 2018, **299**, 172–182.
11 E. B. Pereira and G. A. Martin, *Appl. Catal., A*, 1993, **103**, 291–309.
12 P. de Groot, M. Coulon and K. Dransfeld, *Surf. Sci.*, 1980, **94**, 204–220.
13 G. Greiner and D. Menzel, *J. Catal.*, 1982, **77**, 382–396.
14 M. Agnelli, H. M. Swaan, C. Marquez-Alvarez, G. A. Martin and C. Mirodatos, *J. Catal.*, 1998, **175**, 117–128.
15 M. Agnelli, M. Kolb and C. Mirodatos, *J. Catal.*, 1994, **148**, 9–21.
16 S. Derrouiche and D. Bianchi, *Appl. Catal., A*, 2006, **313**, 208–217.
17 F. C. Meunier, *J. Catal.*, 2019, **372**, 388–388.
18 Y. Zheng, K. Li, H. Wang, Y. Wang, D. Tian, Y. Wei, X. Zhu, C. Zeng and Y. Luo, *J. Catal.*, 2016, **344**, 365–377.
19 R. Atwi, T. Elgayyar, F. C. S. Aires, A. Tuel and F. C. Meunier, *Top. Catal.*, 2021, **64**, 1054–1055.
20 Y. Yao, L. Chen, X. Mao, Y. Yang, J. Chen and L. Zhou, *J. Phys. Chem. C*, 2021, **125**, 8606–8619.
21 R. Atwi, T. Elgayyar, F. J. C. S. Aires, A. Tuel and F. C. Meunier, *Top. Catal.*, 2020, **63**, 1596–1605.
22 F. C. Meunier, I. Dansette, K. Eng and Y. Schuurman, *Catalysts*, 2022, **12**, 793.
23 C.-H. Tu, A.-Q. Wang, M.-Y. Zheng, X.-D. Wang and T. Zhang, *Appl. Catal., A*, 2006, **297**, 40–47.
24 https://harricksci.com/content/Data_Sheet_HVC_High_Temp_Praying_Mantis_Reaction_Chamber.pdf.
25 Y. Jugnet, F. J. C. S. Aires, C. Deranlot, L. Piccolo and J. C. Bertolini, *Surf. Sci.*, 2002, **521**, L639–L644.
26 D. C. Meier, V. Bukhtiyarov and D. W. Goodman, *J. Phys. Chem. B*, 2003, **107**, 12668–12671.
27 P. Hollins, *Surf. Sci. Rep.*, 1992, **16**, 51–94.
28 O. Dulaurent, X. Courtois, V. Perrichon and D. Bianchi, *J. Phys. Chem. B*, 2000, **104**, 6001–6011.
29 K. M. Rao, G. Spoto and A. Zecchina, *Langmuir*, 1989, **5**, 319–325.
30 P. Portius, M. Bühl, M. W. George, F.-W. Grevels and J. J. Turner, *Organometallics*, 2019, **38**, 4288–4297.
31 A. G. Popov, A. V. Smirnov, E. E. Knyazeva, V. V. Yuschenko, E. A. Kalistratova, K. V. Klementiev, W. Grünert and I. I. Ivanova, *Microporous Mesoporous Mater.*, 2010, **134**, 124–133.

 This journal is © The Royal Society of Chemistry 2022